Jurnal Kejuruteraan 37(5) 2025: 2377-2391
https://doi.org/10.17576/jkukm-2025-37(5)-27

Cracks of Can Shells in the Beading Process of Cylindrical Lithium Battery

Bin Luo, Mohamad Hanif M. Saad & Zambri Harun*

Department of Mechanical and Manufacturing Engineering,
Faculty of Engineering and Built Environment, Universiti Kebangsaan Malaysia, UKM Bangi 43600 Malaysia

**Corresponding author: zambri@ukm.edu.my*

Received 23 August 2024, Received in revised form 24 December 2024
Accepted 24 Janaury 2025, Available online 30 August 2025

ABSTRACT

During the assembly phase of cylindrical lithium batteries, the beading process is essential for establishing a support platform required for the installation and sealing of the top cap assembly. This process involves rolling grooves on the battery shell. Despite this, the beading process often results in the formation of cracks in the cylindrical battery can. To this end, endeavors were hereby made to analyze the reasons for the cracks of the beading portion of the 18650-lithium battery can shell. Through the analysis of the microstructure of the can shell and finite element simulation, an in-depth study of the key parameters and series of experiments in the beading process was conducted, summarizing the fundamental causes of cracks in the beading process. The regression analysis result reveals obvious regularity of each influencing factor. The influencing factors in the order of most to least significant are as follows: i. beading knife feeding speed; ii. can thickness; iii. swaging part type; iv. beading holder revolutions speed; and v. beading knife radius (R) and beading knife shape. The feeding speed of the beading knife and the thickness of the can have been identified as significant factors in this study. Optimal process parameters include a beading knife feeding speed of 4.98 mm/s, a can thickness of 0.3 mm at the beading section, a 3-jaw swaging part with a size of 18.2 mm, a holder revolution speed of 1000 RPM, and a beading knife radius & shape of 0.5 (previous specification).

Keywords: Cylindrical lithium batteries; cracks; can shell; beading process; finite element analysis

INTRODUCTION

In response to the evolving landscape of energy storage technology, cylindrical lithium batteries are exhibiting a growth trajectory in size, progressing from the 18650 series to the 46800 and 46950 series. A cylindrical lithium battery typically comprises a cylindrical can, a jelly-roll electrode assembly accommodated in the can, and a cap coupled to an upper portion of the can. The beading portion is designed for cap assembly mounting, while the crimping portion serves to seal the battery. The cylindrical lithium battery features a can shell, referred to simply as a "can." The beading process, also known as the groove rolling process, is utilized to form a support platform on the battery shell by rolling grooves, facilitating the installation and sealing of the top cap assembly. The combination between the battery shell and the top cap assembly is tightened, improving the sealing performance of the battery. It also facilitates to fix the jelly-roll type electrode assembly inside the battery, reduce its displacement and shaking during the battery charging and discharging process, and ensure battery safety. Taking 18650-battery as an example, 18 represents the diameter of the battery, 65 represents the height of the battery, and 0 represents a cylindrical construction, as shown in Figure 1.

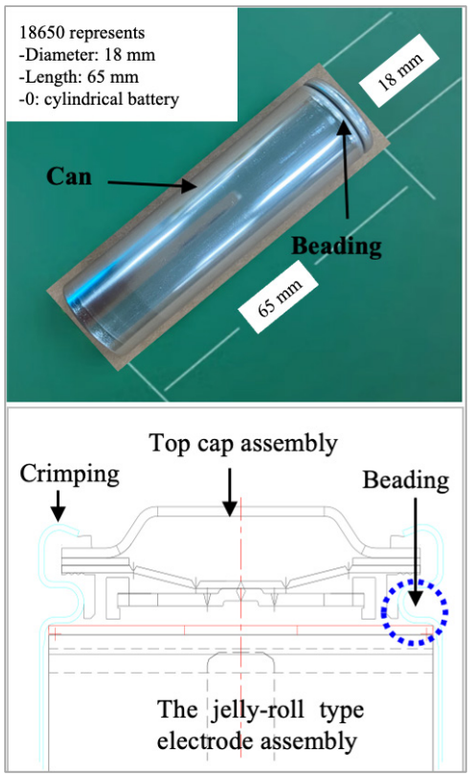

FIGURE 1. Schematic diagram of the 18650 batteries

There are many factors explaining the can shell cracks during the beading process. Zheng et al. (2012) proved that the beading process of cylindrical batteries could be improved by improving the shape and size of the beading knife. It is essential to design an appropriate cam curve and synchronize it with the axial feed movement of the roller cutter to achieve the desired groove formation. The plastic deformation of the material must be considered during production. During the roller groove process, the inner diameter of the groove continues to shrink due to material plastic flow even after the roller cutter ceases radial feeding. This results in an excessively small inner diameter or a thin shell wall, which is influenced by the axial feed movement of the beading knife.

China patent application publication no. CN207071606U provides a new concept to optimize the beading process also by changing the beading knife design. The upper knife edge and the lower knife edge are smoothly connected. The cross-sectional outer contour of the upper knife edge is arc-shaped, while that of the lower knife edge is parabolic. The curvature at any point on the lower knife edge is less than or equal to the curvature of the upper knife edge. Compared to the existing technology, this new beading knife reduces the feeding amount of the lower knife edge, further reducing the stretching amount of the lower notch of the can shell and avoiding cracks caused by the thinness of the wall thickness of the lower notch.

Cui et al. (2015) investigated the causes of tensile ripples during the beading of an 18650-battery, and the results highlighted that: *i*. increasing the can shell thickness at the opening by 0.02 mm not only resolved the beading wave issue but also did not encroach upon the internal space of the battery; *ii* increasing the hardness of the can shell from HRC 42-46 to HRC 48-52 during the heat treatment of cold-rolled can plates enhanced the toughness of the can shell and improved the beading wave; *iii.* the feed amount of the beading knife was decreased by 0.05 mm, relieving the pressure that forced can shell wall deformation and reducing the occurrences of beading wave; *iv.* an oil application was introduced in the beading process. By applying lubricant oil on the can shell, the friction between the beading knife and shell in the beading process was reduced, resulting in more even force distribution and a more stable material flow, thereby preventing the formation of beading waves.

Japanese patent application publication no. JP1999277153 discloses a method of manufacturing a cylindrical member constituting a cathode electrode container in a sodium-sulfur battery. It introduces a technique of performing a beading process while applying pressure in the upper and lower parts. This is to prevent the problem that the thickness of the bead portion is reduced by the beading process, thereby reducing the corrosion resistance and durability.

Korean patent application publication no. KR20090027321A proposes a beading manufacturing method for a cylindrical battery for preventing deformation of a beading portion. The prior art method which involves pressing the top surface of the battery after the crimping process to perform the sizing process, omits the support of the bottom surface of the beading portion during the sizing process, leading to its downward deformation and the formation of the beading portion. A novel beading manufacturing method involves conducting the sizing process simultaneously or continuously with the beading process. This approach allows for more precise control over the width of the beading portion, prevents downward deformation caused by sizing pressure, and consequently, maximizes the internal space, thereby potentially enhancing battery capacity. The beading and sizing processes are performed by an upper spindle mounted on the top of the can, which rotates, and a bead portion support jig capable of vertically moving within the upper spindle. This jig features an adjustable bottom support structure designed to support the bottom surface of the beading portion during the sizing process. The battery can is fixed by an upper spindle and a lower spindle including a bead supporting jig. As the upper and lower spindles rotate, the bead supporting jig in the upper spindle is unfolded by the rotational force, and the beading knife moves forward to

form the beading portion. During the retraction of the beading knife, with the upper and lower spindles in rotation, the beading unit support jig braces the lower surface of the beading part. Concurrently, the upper spindle descends to press and size the beading part. Upon completion of the sizing process, the rotation of the upper and lower spindles is halted. Subsequently, the bead support jig is restored to its original state, the upper spindle is raised, and the lower spindle is lowered.

Over the past years, there have been many studies on the beading process, yet the can shell cracks caused by the beading process have been rarely explored. Table 1 lists several different research directions from 2010 to 2024. According to Table 1, the seven fields of can molding technology and beading process mechanics analysis, beading manufacturing method innovation, and no beading battery structure design innovation are frequently investigated research directions.

TABLE 1. Summary of some research literature on cylindrical lithium battery beading process

No.	Reference	Main research directions						
		Can Forming process	Mechanical analysis of beading process	Beading knife design	Beading Process parameter	Can shell Size/ Material	Beading manufacturing method	No beading battery structure
1	Chen et al. (2023)	o	o	x	x	x	x	x
2	Eve Energy Co., Ltd. (2024)	x	x	x	o	x	o	x
3	Guangdong Nuo Da Smart Energy Technology Co., Ltd. (2023).	x	x	x	o	x	o	x
4	Hao et al. (2016)	x	x	x	x	o	x	x
5	Li et al. (2012)	x	x	x	x	o	x	x
6	Li et al. (2020)	o	o	x	x	x	x	x
7	LG Chem, Ltd. (2017a, 2017b)	x	x	x	o	x	o	x
8	LG Energy Solution, Ltd. (2024a, 2024b)	x	x	x	o	x	o	x
9	LG Energy Solution, Ltd. (2015)	x	x	x	o	x	o	x
10	LG Energy Solution, Ltd. (2020)	x	x	x	x	x	x	o
11	Min et al. (2022)	o	x	x	x	x	x	x
12	Ren et al. (2022)	o	o	x	x	x	x	x
13	Sun et al. (2022a, 2022b)	o	o	x	x	x	x	x
14	SAMSUNG SDI Co., Ltd. (2023)	x	x	x	o	x	o	x
15	SAMSUNG SDI Co., Ltd. (2024a, 2024b)	x	x	x	o	x	o	x
16	SAMSUNG SDI Co., Ltd. (2008)	x	x	x	o	x	o	x
17	Wang et al. (2016)	x	o	x	o	x	o	x

The Beading process is not only an issue in battery manufacturing processes. Recently, Luo et al. (2025) performed an experimental study and finite element analysis (FEA) on another critical area, however, on the 21700 series battery. The study was on the bonding performance in 21700 cylindrical lithium battery modules. The result shows that the stress in the center region is lower than that in the circumference region.

BEADING PROCESS DESCRIPTION

The 18650-battery assembly process of a company in Nanjing was taken as the research case. The beading apparatus is equipped with a rotating-type (eight-pockets) CAM structure. The beading process components include an upper holder for rotating and securing the inner side of the open top of the can and the outer surface. This upper holder is positioned within the

sleeve. It involves a lower holder for fixing the lower end of the can, a backup roller for fixing the beading portion of the can, and a beading knife (disk) for extrusion the side of the can to form the beading portion, as shown in Figure 2. The cam angle operation diagram of a beading process in this study is shown in Figure 3. This equipment and drawings are designed by Canon Machinery Co., Ltd., with the drawing number of BAF0497-00000000Z1R1. The summary is as follows: *i.* at a cam angle of 22.5, the can shell begins to load until the can contacts the upper holder at a cam angle of 85.4; *ii.* at a cam angle of 37.5, the lower holder begins to rise and contacts the bottom of the can at cam angle 92.5; *iii.* at a cam angle of 82.5, the beading knife begins to move forward until it contacts the can at cam angle 102.5, at which time, the beading begins; iv. at the same time, at a cam angle of 82.5, the backup roller also begins to move forward until it stops moving forward at a cam angle of 92.5 and contacts the can at a cam angle of 107.2. *v.* at a cam angle of 180, the upper holder begins to press down, and the lower holder continues to rise, during which, the beading knife continues to move forward; *vi.* at a cam angle of 197.5, the beading knife stops moving forward. Until the cam angle reaches 187.5, the upper holder stops pressing down, and at a cam angle of 202.5, the lower holder stops rising. So far, the beading process is completed. At the cam angle of 217.5, the beading knife and the backup roller begin to retreat. The lower holder and the upper holder also successively detach from the can.

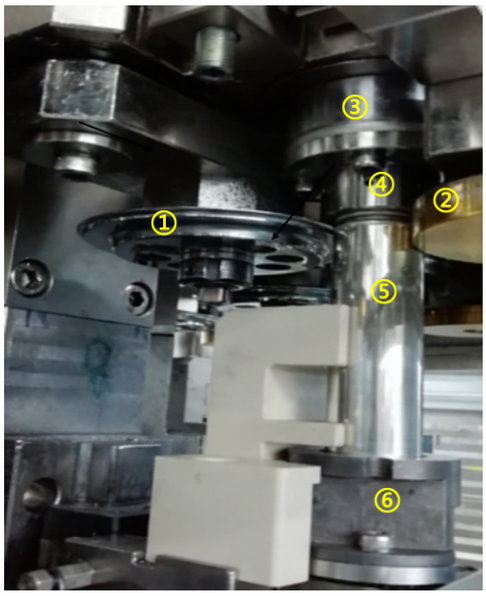

FIGURE 2. Schematic diagram of a beading machine ① Beading knife (disk); ② Back up Roller; ③ Sleeve; ④ Upper holder (head); ⑤ Can shell; ⑥ Lower holder (head)

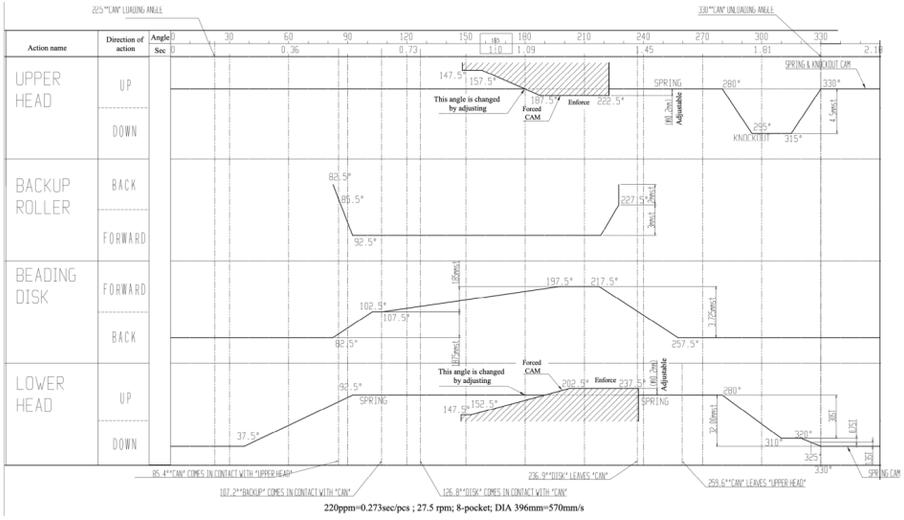

FIGURE 3. The CAM angle operation diagram of a beading process

In the beading process of the assembly stage, cracks frequently occur in the groove of can shells. Crack formation in the can shells can lead to electrolyte leakage, posing a significant safety hazard and adversely affecting battery performance. Two crack samples (numbered 1 and 2) are shown in Figure 4. The samples in Figure 4 were sourced from a company base in Nanjing, China. The test samples were commissioned by FUDA Analytical Testing Group for testing and provided accompanying pictures and other information.

Observing the cracks morphology under a lectern microscopy, it was found that the can shell corresponding to the cracks position produced large stress and plastic deformation, and beading waves were formed. The cracks were located at the groove of rolling extrusion molding. The cracks extended longitudinally, with a larger opening on the inner surface and a smaller opening on the outer surface. The outer surface of the groove displayed numerous sliding marks resulting from processing friction.

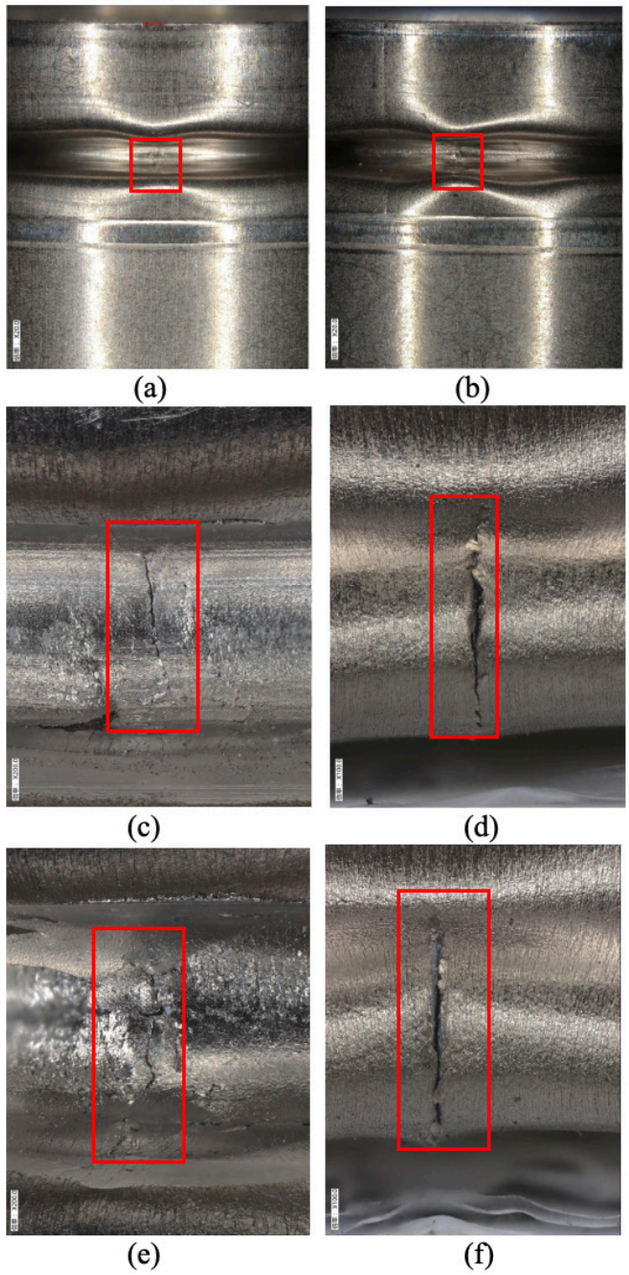

FIGURE 4. Morphology of can shell cracks samples

(a) morphology of the outer side of the groove of cracks sample No. 1 (X20); (b) morphology of the outer side of the groove of cracks sample No. 2 (X20); (c) morphology of the outer side of the groove of cracks sample No. 1 (X200); (d) morphology of the inner side of the groove of cracks sample No. 1 (X100); (e) morphology of the outer side of the groove of cracks sample No. 2 (X200); and (f) morphology of the inner side of the groove of cracks sample No. 2 (X100).

MATERIALS AND METHODOLOGY

The main approach of this investigation was to conduct the finite element simulation, an in-depth study of the key parameters and series of experiments in the beading process was conducted, summarizing the fundamental causes of cracks in the beading process.

The significant factors included can shell design thickness, beading knife dimension, design shape, equipment parameter etc. Unigraphics NX software was employed to complete the can geometrically model. To measure and fit the can shell material, a bi-linear isotropic hardening constitutive model was employed. ABAQUS software was utilized for the simulation analysis. Minitab software was used for regression analysis, and the correlation of the factors was assessed using the PEEQ (Plastic Equivalent Elastic Strain).

The can plate material of the 18650 battery consists of SPCC can plates with thicknesses of 0.3 mm. Here, SPCC stands for S-Can, P-Plate, C-Cold, and C-Common. The can shell undergoes a pre-nickel-plating process. The thickness of the external nickel plating is 3 μm, while that of the internal nickel plating is 2 μm. According to the product specification requirements, the thickness changes of various parts of the can plate substrate after being stretched and formed by the can shell process, and details are shown in Figure 5.

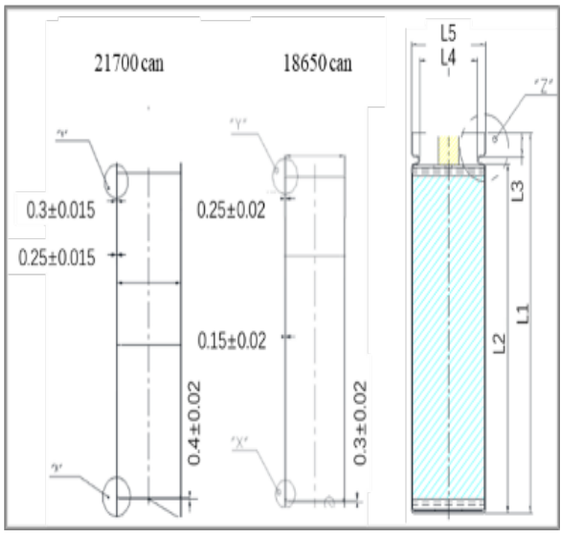

FIGURE 5. Can shell dimension

RESULTS AND DISCUSSION

CRACKS MICROSTRUCTURE ANALYSIS

In this study, the test samples were commissioned by a Korean institution and equipment's for testing. Normal sample No. 1 and cracked sample No. 1 were cut, inlaid, ground, and polished, and the transverse and longitudinal cross-sectional morphologies of the beading area were observed. It was found that the nickel-plating layer in cracked sample No. 1 had penetrated the substrate, as shown in Figure 6(a), especially at the crack, where a nickel-plating layer was found on the fracture, as shown in Figure 6(b). The presence of a nickel-plating layer at the fracture indicated that the nickel-plating layer penetrated the substrate, and cracks existed before or during plating. Observation of normal samples also revealed that the nickel-plating layer penetrated the substrate, as shown in Figure 6(c).

Comparison analysis of the microscopic structures of cracks and normal samples indicates pre-existing micro-cracks prior to nickel plating. This precludes the conclusion that micro-cracks are the predominant factor in can shell cracking post-beading.

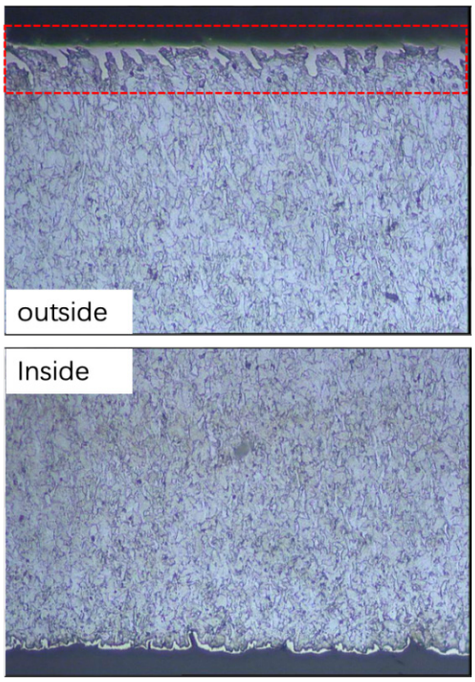

(a) Transverse section metallographic structure of cracks sample No. 1

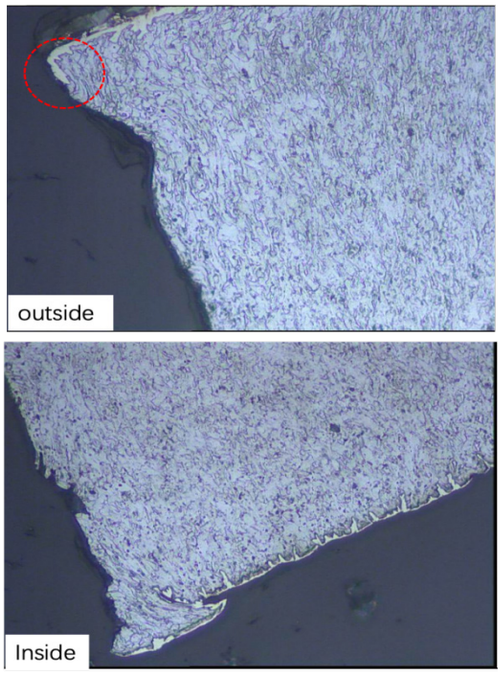

(b) Transverse section metallographic structure of fracture of cracks sample No. 1

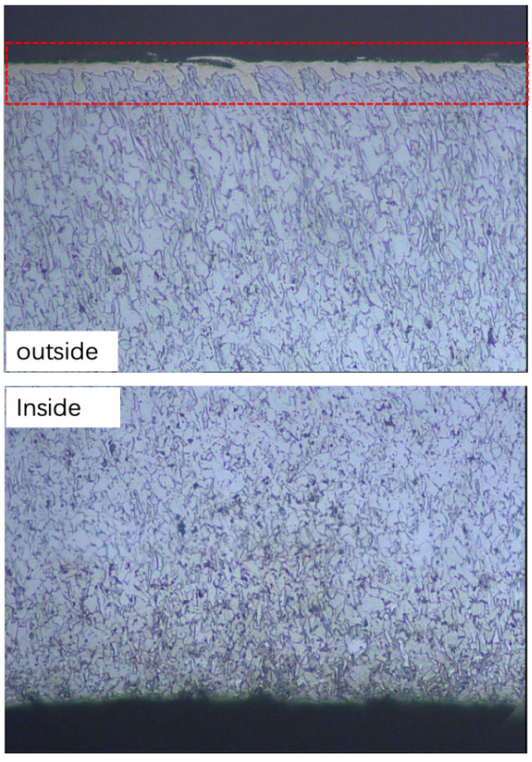

(c) Transverse section metallographic structure of normal sample No. 1

FIGURE 6. Metallographic structure of cracks sample No. 1 and normal sample No.1 (X500)

Further three cracks' batteries numbered 3-5 were hereby selected for cross-sectional analysis. The results show that cracks position average thickness 316.5 μm is 22% larger than the average thickness of non-cracks position average 260 μm, as detailed in Table 2. The cross-section image of the No. 3 cracks sample is shown in Figure 7. It is speculated that beading extrusion continues after the cracks occurs. The greater the thickness deviation after beading, the higher the risk of cracks. Reducing thickness variation post-beading is crucial for mitigating the risk of crack formation.

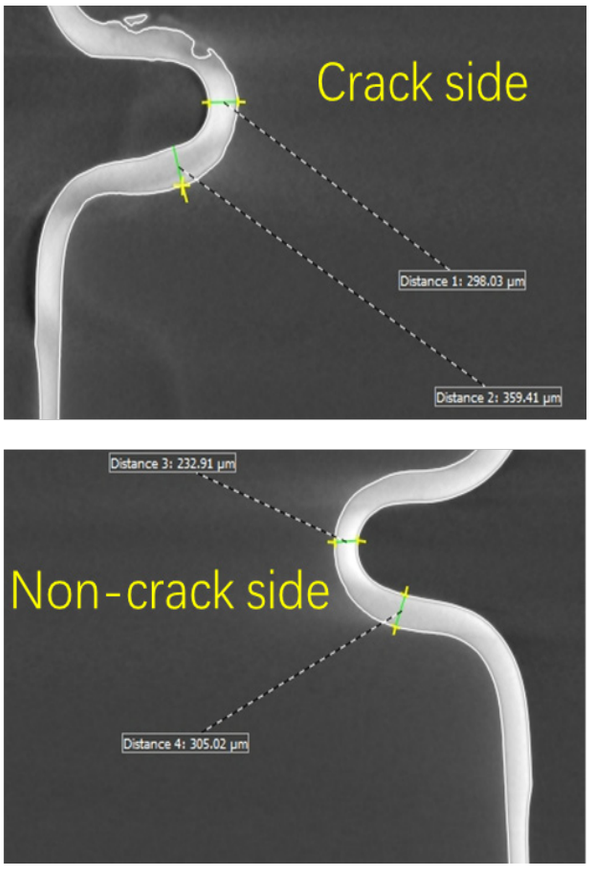

FIGURE 7. Cross-sectional image of No. 3 cracks sample

TABLE 2. Comparison of cracks sample thickness (unit: μm)

Sample	Cracks side	Cracks side average	Non-cracks side	Non-cracks side average
No. 3	299	316	224	259
	328		271	
No. 4	298		233	
	359		305	
No. 5	254		233	
	357		288	

FINITE ELEMENT ANALYSIS

Further finite element simulation analysis was conducted on the key parameters of the beading process, and experimental design was carried out. The significant factors included can shell design thickness, beading knife dimension, and design shape, and equipment parameters etc., which were hereby combined. To demonstrate the correlation between equipment parameter factors and cracks.

PEEQ stands for Equivalent Plastic Strain, a metric employed in plasticity analysis to quantify the total plastic strain experienced by a material throughout its plastic deformation. A PEEQ value exceeding zero indicates material yielding, reflecting the aggregate effect of plastic strain over the entire deformation process. Therefore, in this stage, based on the selected factor, a simulation for each factor was hereby performed to check the PEEQ. Statistical analysis was carried out through a total of 18 groups (2 levels – 1 factor / 3 levels – 4 factors) orthogonal experimental design. The contribution rate analysis of sensitive factors of machine parameters was completed by evaluating the PEEQ, with smaller PEEQ values indicating better performance. The goal was to identify the optimal process conditions.

The analysis in this project focused on the 18650-battery can shell. Unigraphics NX software was employed to complete the can geometrically model, The model is primarily composed of the upper holder, can shell, beading knife, etc., as shown in Figure 8. Regarding the material properties of the battery can shell, a total of 8292 data points were measured, and the test data are shown in Figure 9(a). However, during the battery can shell beading process, the material entered the large deformation stage, so a bilinear isotropic hardening constitutive model with plasticity was adopted, ignoring the later unloading and plastic deformation stages. Besides, a bilinear model was employed. The fitting curve is shown in Figure 9(b). In the first stage, namely the linear elastic stage, the maximum yield strength is 316.5MPa, and the tangent modulus in the second stage is 737.7MPa. The material properties were processed by Excel using piecewise linear regression, with the goodness of fit of the two stages being 0.94 and 0.95, respectively. The parameters of can shell material at room temperature are shown in Table 3.

TABLE 3. Parameters of can shell material

Tangent modulus (MPa)	Poisson' Ratio	Density (ton/mmΛ3)	Yield Strength (MPa)
737.71	0.3	7.92E-09	371

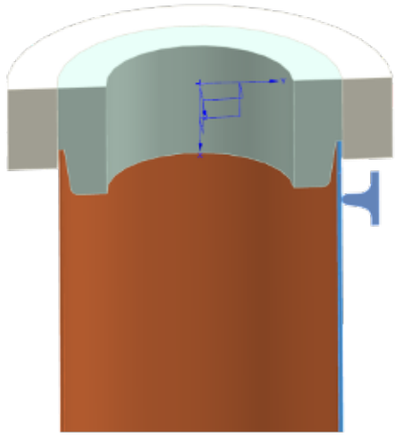

FIGURE 8. Simulation Model

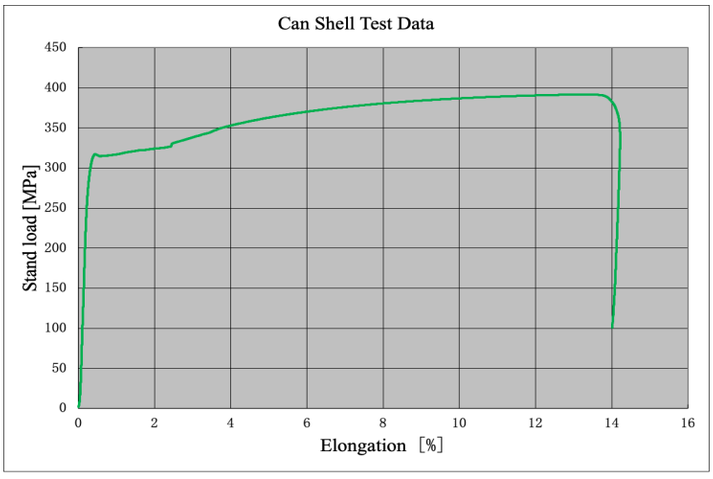

(a)

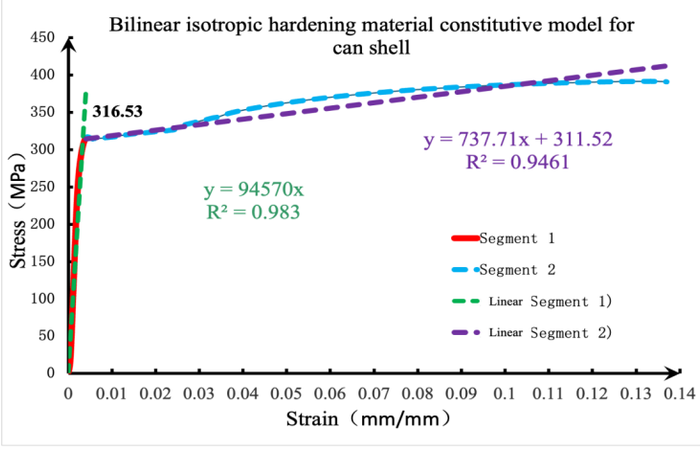

(b)

FIGURE 9. (a) Experimental stress–strain data obtained from 8,292 measurements of the battery can shell material. (b) Fitted bilinear isotropic hardening model used to characterize the material's plastic behavior during the beading process, capturing the large deformation stage while neglecting unloading and subsequent plastic deformation.

Meshing is a key prelude to CAE simulation, necessitating the generation of surface and volume meshes that meet specific quality standards. However, reasonable simplification of the geometric model impacts both the quality of the calculation mesh and the calculation speed, thereby significantly affecting the accuracy and speed of the simulation. Therefore, the upper holder, can shell, knife, etc. were hereby simplified into 2D axisymmetric units to simulate the battery can shell forming. The meshing method was specified as quadrilateral mesh, with a maximum size of no more than 0.5mm. Orthogonal quadrilateral mesh was used for the battery can shell, four layers of mesh were controlled in the thickness direction, and the contact area with the Beading Knife was controlled by 120 mesh nodes. In addition, the front section of the Beading Knife was controlled by 20 mesh nodes, and attention was paid to the consistency of the contact mesh size, which was controlled within 3 times. The battery can shell had a mixed mesh of about 6557 nodes and 1926 units. After completing the overall and local mesh control, all multi-bodies were meshed immediately. Details are shown in Figure 10.

The contact relationship settings of the holder, beading knife and can on the upper part of the battery can shell are shown in Figure 11, where the upper holder and the upper part of the battery can shell can are in binding contact, the holder and the left side of the battery can shell can are in friction contact, and the beading knife and the right side of the battery can shell can are in friction contact. The friction coefficient is 0.12, and the tolerance for judging contact is set to 0.005 mm, ignoring the influence of gravity.

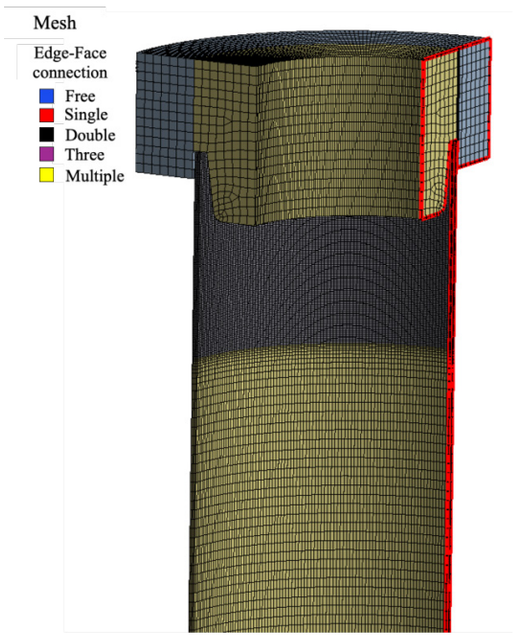

FIGURE 10. Can shell overall mesh effect diagram

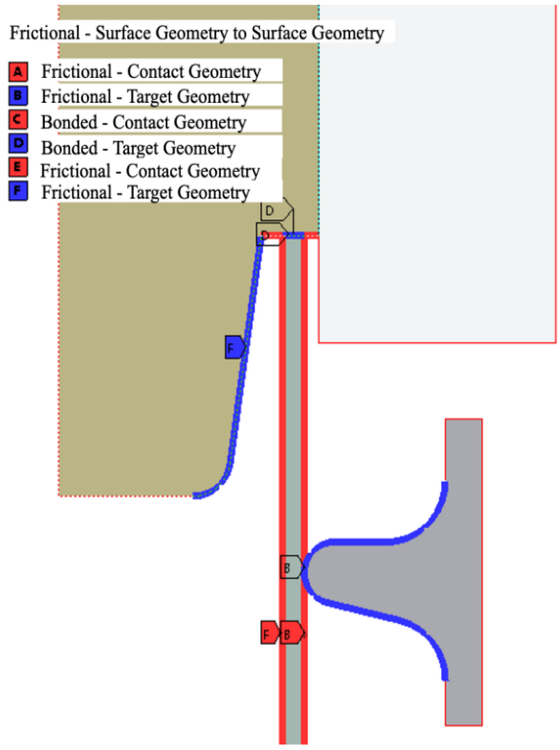

FIGURE 11. Schematic diagram of the contact setting of the can shell boundary condition

Given the high extrusion force applied to the can shell during the swaging process, the swaging part shape is also considered an influencing factor. The purpose of swaging is to extrude the upper part of the can using a 3-jaw or sleeve, which reduces the outer diameter of the can and optimizes the internal space of the can. These two different designs of swaging part type are shown in Figure 12(a). To mitigate cracking, a new beading knife design was hereby intended for implementation on the production line. The two distinct knife shapes are presented in Figure 12(b), and their corresponding radius in Figure 12(c).

A total of 18 groups of parameterized models of the can shell were calculated to obtain its stress and strain. This study examined the influence of the beading knife radius and shape, holder rotation speed, beading knife feed speed, can shell swaging part shape, and can shell thickness on its stress and strain. Experimental design factor and parameter level are shown in Table 4.

The simulation analysis result is shown in Table 5. The contribution rate analysis of sensitive machine parameter factors, evaluated using PEEQ, is depicted in Figures 13 and 14.

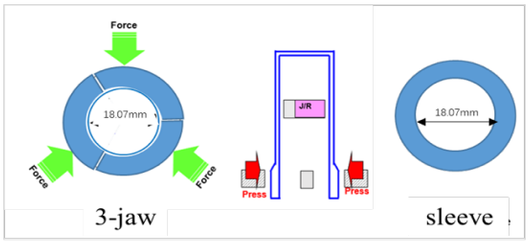

(a) Difference of swaging part type & size.

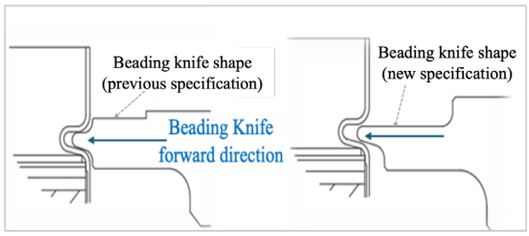

(b) Difference of beading knife shape and radius.

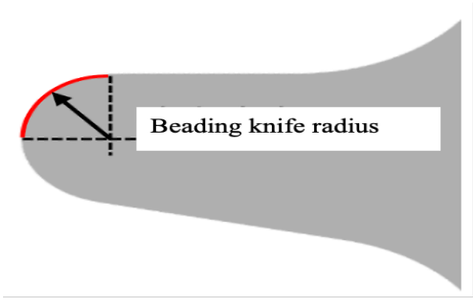

(c) Difference of beading knife radius

FIGURE 12. (a) Two different swaging part designs used to optimize internal space by reducing the can shell's outer diameter during the high-force swaging process. (b) Comparison of two beading knife shapes proposed to mitigate cracking during forming. (c) Corresponding radii of the two knife designs.

TABLE 4. Experimental design factor and parameter level

	Key factors	Parameter level		
Factors (x's)	Can thickness (beading portion)	0.25 mm	0.3 mm	-
	Beading knife Radius (R)/shape	R 0.4 mm/ previous specification	R 0.5 mm/ previous specification	R 0.5 mm/ new specification
	Upper holder revolution speed	1000 RPM	800 RPM	1200 RPM
	Beading knife feeding speed	4.98 mm/sec	3.36 mm/sec	4.84 mm/sec
	Swaging part type	3-jaw/18.12 mm	3-jaw/18.07 mm	Sleeve/18.07 mm
Responses (y)	Equivalent plastic strain (PEEQ)			

*Remark: RPM refers to Rotations Per Minu

TABLE 5. Experiment set (L18 orthogonal array) and results

No.	Can thickness (mm)	Beading knife R/shape (mm)	Upper holder revolution speed (RPM)	Beading knife feeding speed (mm/sec)	Swaging part type (mm)	PEEQ
1	0.25	R0.4/ (previous specification)	1000	4.98	3-jaw / 18.12	1.367
2	0.25	R0.4/ (previous specification)	800	3.36	3-jaw / 18.07	1.687
3	0.25	R0.4/ (previous specification)	1200	4.84	Sleeve / 18.07	1.373
4	0.25	R0.5/ (previous specification)	1000	4.98	3-jaw / 18.07	1.181
5	0.25	R0.5/ (previous specification)	800	3.36	Sleeve / 18.07	1.742
6	0.25	R0.5/ (previous specification)	1200	4.84	3-jaw / 18.12	1.43
7	0.25	R0.5/ (new specification)	1000	3.36	3-jaw / 18.12	1.625
8	0.25	R0.5/ (new specification)	800	4.84	3-jaw / 18.07	1.306
9	0.25	R0.5/ (new specification)	1200	4.98	Sleeve / 18.07	1.335
10	0.3	R0.4/ (previous specification)	1000	4.84	Sleeve / 18.07	1.297
11	0.3	R0.4/ (previous specification)	800	4.98	3-jaw / 18.12	1.362
12	0.3	R0.4/ (previous specification)	1200	3.36	3-jaw / 18.07	1.477
13	0.3	R0.5/ (previous specification)	1000	3.36	Sleeve / 18.07	1.486
14	0.3	R0.5/ (previous specification)	800	4.84	3-jaw / 18.12	1.313
15	0.3	R0.5/ (previous specification)	1200	4.98	3-jaw / 18.07	1.203
16	0.3	R0.5/ (new specification)	1000	4.84	3-jaw / 18.07	1.293
17	0.3	R0.5/ (new specification)	800	4.98	Sleeve / 18.07	1.29
18	0.3	R0.5/ (new specification)	1200	3.36	3-jaw / 18.12	1.602

General linear model

一般线性模型: PEEQ 与 Can thicknes, Beading knif, Upper holder, Beading knif, Swaging part

方法

因子编码 (-1, 0, +1)

因子信息

因子	类型	水平数	值
Can thickness	固定	2	0.25, 0.30
Beading knife R/shape	固定	3	0.4, 0.5/old, 0.5/new
Upper holder revolution speed	固定	3	800, 1000, 1200
Beading knife feeding speed	固定	3	3.36, 4.84, 4.98
Swaging part type	固定	3	Jaw/18.12, Jaw/18.07, Sleeve18.07

p-value

Variance analysis

来源	自由度	Seq SS	分布	Adj SS	Adj MS	F 值	P 值
Can thickness	1	0.029041	6.48%	0.029041	0.029041	8.42	0.020
Beading knife R/shape	2	0.003612	0.81%	0.003612	0.001806	0.52	0.611
Upper holder revolution speed	2	0.017280	3.86%	0.017280	0.008640	2.51	0.143
Beading knife feeding speed	2	0.344205	76.79%	0.344205	0.172102	49.92	0.000
Swaging part type	2	0.026503	5.91%	0.026503	0.013252	3.84	0.068
误差	8	0.027579	6.15%	0.027579	0.003447		
合计	17	0.448220	100.00%				

模型汇总

S	R-sq	R-sq (调整)	PRESS	R-sq (预测)
0.0587147	93.85%	86.92%	0.139620	68.85%

FIGURE 13. Regression analysis results

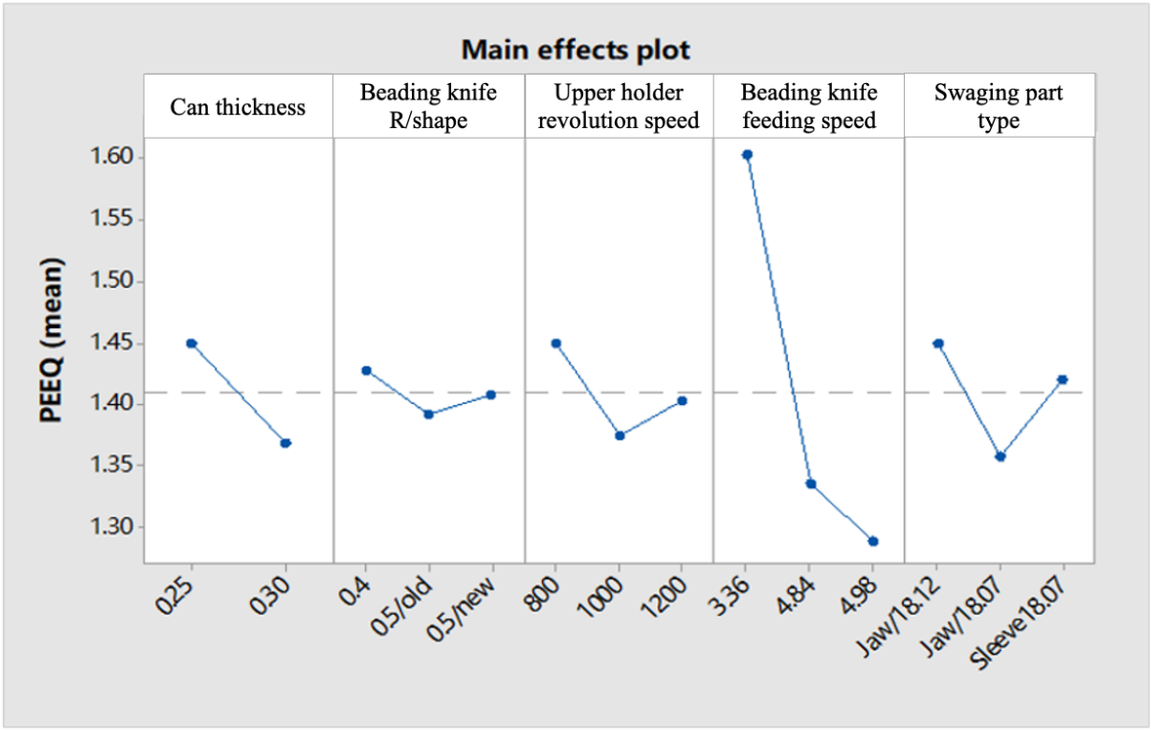

FIGURE 14. Main effects plot of PPEQ

CONCLUSION

This paper demonstrates that the most important beading parameter of the can shell in 18650-cylindrical lithium battery assembly stage can be determined using combined experimental design and simulation methods. The effect of pre-existing micro-cracks prior to nickel plating is analyzed using metallographic analysis and visual analysis. Comparison analysis of the microscopic structures of failed and normal samples indicates pre-existing micro-cracks prior to nickel plating. This precludes the conclusion that micro-cracks are the predominant factor in can shell cracking post-beading. The reasons for the cracks of beading portion were hereby investigated through stress and strain simulation. The contribution rate analysis of sensitive factors of machine parameters was completed by evaluating the PEEQ. The regression analysis results indicate clear patterns for each influencing factor. The influencing factors in the order of most to least significant include *i.* beading knife feeding speed; *ii.* can thickness; *iii.* swaging part type; *iv.* beading holder revolutions speed; and *v.* beading knife radius and beading knife shape. Only the beading knife feeding speed and can thickness be considered significant factors. This study holds considerable significance in reducing the defect rate. According to the results, the optimal process parameter combination involves a beading knife feeding speed of 4.98 mm/s, a can thickness of 0.3 mm in beading portion, a swaging part type 3-jaw of 18.2 mm, a holder revolution speed of 1000 RPM, and a beading knife radius & shape of 0.5 (previous specification).

ACKNOWLEDGEMENT

Our sincerest gratitude is extended to the company that facilitated the detailed experimentation and simulations, provided the testing platform, and covered the associated costs. Thanks are also due to Chen, Ling, Seungtae Lee, Jaeson Shin, and Moon Jun-ho for their valuable suggestions. Additionally, appreciation is expressed for the research university grant GUP-2024-058 from UKM.

DECLARATION OF COMPETING INTEREST

None.

REFERENCES

Cui, S. H., Zhang, L. H., & Sun, Z. H. 2015. Based on the theory of TRIZ solving the problem of 18650 battery beading waves. P The 17th Annual Conference of the China Association for Science and Technology. Guangzhou, May 23, 2015.

Chen, T. F., L, S. C., Zhu, F.Q., Zhao, H. C.， Zhao, P. B. 2023. Finite element simulation for can case's shrinking technic of lithium battery. *Modern Manufacturing Technology and Equipment* (03): 158-161.

Dongguan Chuang Ming Battery Technology Co., Ltd. 2018. Cylindrical battery hobbling cutter CN207071606U.

Eve Energy Co., Ltd. 2024. Rolling method and rolling device for cylindrical battery. CN117816809A.

Guangdong Nuo Da Smart Energy Technology Co., Ltd. 2023. Inverted channeling method for cylindrical battery. CN115739991A.

Hao, Y.H., Chen, J., & Jiao, M. 2016. Design of high specific energy lithium-ion battery casing. *Power Sources Technology* 40(8): 3.

Li, W., Pan Y., Zhang M. J., Zhou Z.F., Du Y.Y., & Hui J.K. 2012. Corrosion resistance of nickel-cobalt alloy plated can strip and lithium battery can shell made of it. *Materials Protection* 45(2): 4.

Li, Y. Y. 2020 Research on multistep drawing of power battery can shell for new energy automobile. Master's thesis, Anhui University of Technology, Anhui, China.

LG Chem, Ltd. 2009. Process for preparing cylindrical battery to prevent deformation of beading portion. KR20090027321A.

LG Chem, Ltd. 2017. Cap Assembly and second battery using same. EP2626925B1.

LG Chem, Ltd. 2017. Secondary battery and manufacturing method for secondary battery. KR20170107741A.

LG Energy Solution Co., Ltd. 2020. Cylindrical battery having. no beading part. EP3584853A4.

LG Energy Solution, Ltd. 2024. Battery cell fixing device and electrolyte impregnation device including the same. US20240014532A1.

LG Energy Solution, Ltd. 2015. Secondary battery and method for manufacturing the same. US20150004446A1.

LG Energy Solution, Ltd. 2024. Cylindrical battery beading equipment and beading method. KR20240087578A.

Luo, B., Md Saad, M. H., Molla A. H. & Harun, Z. 2025. Optimization and analysis of ultrasonic wedge bonding parameters for enhanced bonding performance in 21700 cylindrical lithium battery modules, Pertanika Journal of Science & Technology, 33(3): 1483-1507.

Min, J. C. 2022. Research on forming technology of battery shell. *Forging and Stamping* (02): 37-42.

NGK Insulators Ltd. 1999. Formation of constriction to cylindrical member. JP1999277153.

Ren, Z. B., Cao, C. P. 2022. Optimization of the first deep drawing process parameters for power battery shell based on entropy weight comprehensive evaluation method. *Chinese Mechanical Engineering* 33(13):1622-1628.

Sun, W. 2022. Deep drawing technology and numerical simulation of cylindrical battery shell. Doctoral dissertation, Hefei University of Technology, Hefei, China.

Sun, W., Tian W. C., Ji, X. H., Xue, K. M. 2022. Influence of process parameters on deep drawing of cylindrical battery cases. *Forging and Stamping* (20):23-26.

SAMSUNG SDI Co., Ltd. 2024. Rechargeable battery and manufacturing method thereof. US20240258615.

SAMSUNG SDI Co., Ltd. 2024. Battery pack. US20240322344.

SAMSUNG SDI Co., Ltd. 2023. Cylindrical secondary battery. EP4210157A1.

SAMSUNG SDI Co., Ltd. 2008. Secondary battery and method of manufacturing the same: US7364817B2.

Wang, S. R. 2016. Virtual prototype design of roll groove machine applied for cylindrical lithium battery. Master's thesis, Harbin University of Commerce, Harbin, China.

Zheng, Y. Y., Fu, C. B., Sun, M. & Xu, Q. Z. 2012. Improving of beading process for column Li-ion battery. *Battery Bimonthly* 42(06): 343-345.